Supplementary materials

Text S1 Raw materials

The peanut shell was cleaned multiple times with distilled water before baking at 80℃ for at least 12 h. After crushing the dried peanut shell with a micronizer (Royalstar, RS-FS1811, China), the powder was sieved to obtain a fine powder (100 mesh). The raw bentonite and dolomite were obtained from Hongyao Mine Product Processing Plant in Lingshou Country, Hebei Province, China. Table S1 shows the properties of bentonite and dolomite. Chemically pure PVC, NMP, KH_2PO_4, HNO_3, NaOH, NaCl, KCl, K_2SO_4, KNO_3, KF, $KHCO_3$, HA, BSA and all other chemicals were analytical grade. They were supplied by China's Sino pharm Chemical Reagent Co., Ltd. Dry KH_2PO_4 was dissolved to prepare a phosphate stock solution of 1000 mg/L.

Text S2 Adsorption performance evaluation, kinetics and isotherms

The equilibrium adsorption capacity (q_e, mg/g), adsorption capacity at time t (q_t, mg/g) and removal efficiency (%) were calculated by using the formulae below:

$$q_e = \frac{(C_0 - C_e)V}{W} \quad , \qquad \text{(S1)}$$

$$q_t = \frac{(C_0 - C_t)V}{W} \quad , \qquad \text{(S2)}$$

$$\textit{Removal efficiency}\ (\%) = \frac{(C_0 - C_t)}{C_0} \times 100\% \quad , \qquad \text{(S3)}$$

where C_0 (mg/L), C_e (mg/L), and C_t (mg/L) were initial phosphate concentration, equilibrium phosphate concentration and phosphate concentration at time t (h), respectively, V (L) is the solution volume, and W (g) is the DO/BB weight.

The kinetic experiments were performed by adding 1.6 g DO/BB to 1000 mL 50 mg/L phosphate solution. The phosphate concentrations were determined at different times. To understand the mechanisms of adsorption kinetics, the experimental data were fitted with the following five kinetic models:

Pseudo-first-order model:

$$q_t = q_e - q_e e^{-k_1 t} \quad , \qquad \text{(S4)}$$

Pseudo-second-order model:

$$q_t = \frac{k_2 q_e^2 t}{1+k_2 q_e t} \quad , \qquad \text{(S5)}$$

Richie nth-order model:

$$q_t = q_e \left\{ 1 - \left[\frac{1}{\beta + k_n (n-1) t} \right]^{1/n-1} \right\} \quad , \qquad \text{(S6)}$$

Elovich model:

$$q_t = \frac{1}{\beta} ln(\alpha \beta t) \quad , \qquad \text{(S7)}$$

Intraparticle diffusion model:

$$q_t = k_{id} t^{0.5} + C \quad , \qquad \text{(S8)}$$

where k_1 (1/min), k_2 (g/mg/min) and k_n (g^{n-1}/mg^{n-1}/min) are the pseudo-first-order equilibrium rate constant, pseudo-second-order equilibrium rate constant and Ritchie nth-order equilibrium rate constant, respectively; α (mg/g/min) is the adsorption rate at initial time, while β (g/mg) denotes the constant of desorption. k_{id} (mg/g/h$^{0.5}$) is the rate constant of intraparticle diffusion and C (mg/g) is determined by the thickness of boundary layer.

The isotherm experiments were performed by adding 64 mg DO/BB to 40 mL different phosphate solutions (initial concentrations of 50, 100, 150, 200, 250 and 300 mg/L) and shaken for 24 h to reach equilibrium. Subsequently, the solid was separated and the phosphate concentration in solution was measured. The data were fitted with four isotherm models including Langmuir, Freundlich, Langmuir_Freundlich and Temkin listed below:

Langmuir model:

$$q_e = \frac{q_m K_L C_e}{1+K_L C_e} \quad , \qquad \text{(S9)}$$

Freundlich model:

$$q_e = K_F C_e^n \quad , \qquad \text{(S10)}$$

Langmuir_Freundlich model:

$$q_e = \frac{K_{LF} q_m C_e^n}{1+K_{LF} C_e^n} \quad , \qquad \text{(S11)}$$

Temkin model:

$$q_e = \frac{RT}{B} \ln(AC_e) \quad , \qquad \text{(S12)}$$

where K_L (L/mg), K_F (mg$^{(1-n)}$·L^n/g) and K_{LF} (L^n/mg^n) are the Langmuir adsorption equilibrium constant determined based on the affinity and free energy of the adsorption process, the affinity parameters of Freundlich and Langmuir-Freundlich, respectively; q_m (mg/g) indicates the Langmuir maximum adsorption capacity; n is the Freundlich linearity constant, while B (J·g/mg) and A (L/mg) are the Temkin model constants.

Text S3 SEM and EDS analysis

The SEM images of BB900, DO900 and DO/BB are shown in Fig. S2. As can be seen from Figs. S2(a1), S2(b1) and S2(c1), the surfaces of BB900 and DO900 are relatively rough, while that of DO/BB is relatively flat. This may be attributed to the uniform distribution of pyrolyzed dolomite on the biochar surface. The higher resolution images (Figs. S2(a2), S2(b2) and S2(c2)) reveal no significant difference in the surface morphologies of the three samples. The highest resolution image shows that BB900 presents a loose and porous structure (Fig. S2(a3)). DO900 contains multiple stacked nanoparticles (Fig. S2(b3)), possibly the products generated by dolomite pyrolysis decomposition, MgO and CaO. DO/BB shows a uniform dispersion of nanoparticles, possibly similar to MgO and CaO uniformly dispersed on the biochar surface.

EDS mapping results and element composition of BB900, DO900 and DO/BB are shown in Fig. S2 and Table S2 respectively. Following biomass and bentonite co-pyrolysis, the main elements were C, O, Si and Al, due to the biomass carbonization and some functional groups, in addition with SiO2, Al2O3 and some exchangeable cation (Ca^{2+} and Mg^{2+}) of bentonite. The molecular formula of dolomite is $CaMg(CO_3)_2$. After pyrolysis, the levels of Ca, Mg and O were 62.74%, 3.14% and 30.15% respectively, while that of C was only 3.08%, indicating that dolomite was decomposed sufficiently at the pyrolysis temperature of 900℃. The main elemental composition of DO/BB was: C (7.36%), O (43.74%), Ca (32.61%) and Mg (15.81%). However, the Si and Al levels were reduced significantly, suggesting that the addition of bentonite catalyzed the thermal decomposition of dolomite and greatly increased the MgO content.

Text S4 BSA rejection experiment

Bovine serum protein (BSA) is a typical biological macromolecule in water. BSA was selected for the interception in this study to explore the interception properties of different UF membranes. The calculated BSA interception is an important index for evaluating the membrane performance. The phosphate buffer solution was prepared as follows: First, 3.007 g Na_2HPO_4 and 0.218 g KH_2PO_4 were fully dissolved in 1 L of DI water, followed by the addition of 200 mg BSA. The solution was used for filtration. The UF membrane was fixed in the ultrafiltration device with an effective membrane diameter of 5 cm. Pressurized by 0.1 MPa, a 100 mL filtration solution flowed through the UF membrane. The absorbance of the initial and penetrated solution was determined at 279 nm using a UV-Vis spectrophotometer. The BSA rejection (R, %) was calculated as follows:

$$R=(1-\frac{C_f}{C_i})\times 100\% \quad , \qquad \text{(S13)}$$

where C_i (mg/L) is the concentration of BSA in the initial solution, and C_f (mg/L) is the concentration of BSA in penetrated solution.

The BSA rejection of pure PVC membrane was only 12%, which is due to the presence of numerous pores inside the membrane that facilitate BSA penetration. With the addition of DO/BB, the BSA rejection increased significantly to 73%, 81%, and 85% for PVC-10%DO/BB, PVC-15%DO/BB and PVC-20%DO/BB, respectively. This is due to the addition of DO/BB disrupting the "finger-like" porous structure of PVC membrane and filling the inner membrane pores, which effectively intercepted organic macromolecules such as BSA. Pore size distributions of PVC and PVC-20%DO/BB are shown in Fig. S4 in SM. The pore size of PVC membrane was essentially 80–100 nm and that of PVC-20%DO/BB was concentrated at 40–60 nm. The pore size was consistent with our speculation. The above results indicate that the addition of DO/BB has significantly improved the BSA rejection properties of PVC membranes, thus enabling the dual functions of adsorption and ultrafiltration.

Text S5 Kinetic and isotherm analysis

The phosphate adsorption kinetics is presented in Figs. 6(a) and 6(b), and the corresponding parameters are shown in Table S3. Table S3 shows that the Elovich model can better fit the data (R^2 of 0.9921), indicating that chemisorption on the heterogeneous surface of DO/BB was the dominant force for the adsorption process (Luo et al., 2021). Further, the intraparticle diffusion model was also used for experimental data fitting. The k_{i1} value was 21.31 mg/g/h$^{0.5}$, indicating a high adsorption rate due to the external diffusion (Deng et al., 2021). The k_{i2} of 4.22 mg/g/h$^{0.5}$ suggests intraparticle or pore diffusion process. The k_{i3} of 1.07 indicates adsorption tending to equilibrium.

Adsorption isotherm fitting was used to illustrate the mechanisms. The fitting curves for the Langmuir, Freundlich, Langmuir_Freundlich and Temkin models are shown in Fig. 6(c), and the parameters are listed in Table S4. As can be seen in Fig. 6(c), when the initial phosphate concentration increased from 50 to 300 mg/L, the phosphate removal performance of DO/BB also increased. The R^2 of Temkin model was the highest (0.9950), indicating that the adsorption sites were not homogeneous. Thus, multiples mechanisms regulate the phosphate adsorption (Klimaviciute et al., 2010).

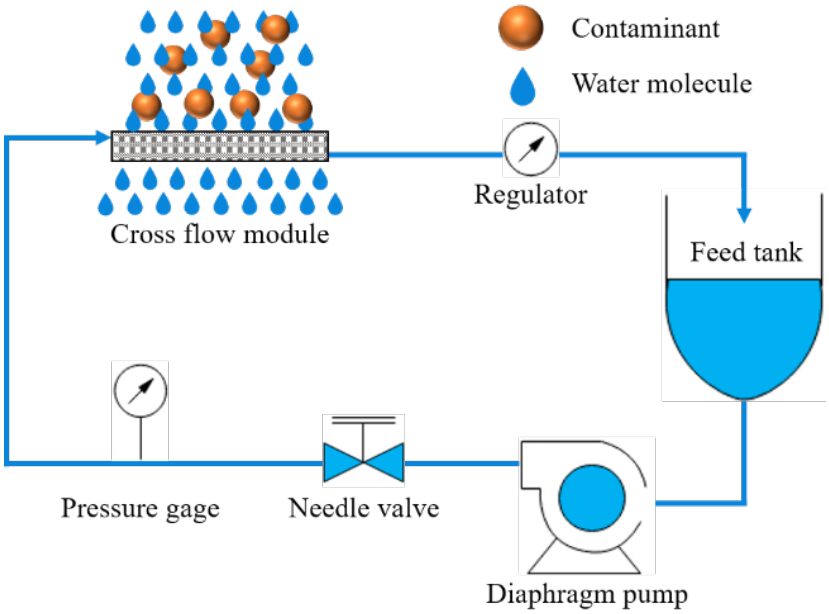

Fig. S1 schematic diagram of the crossflow UF system.

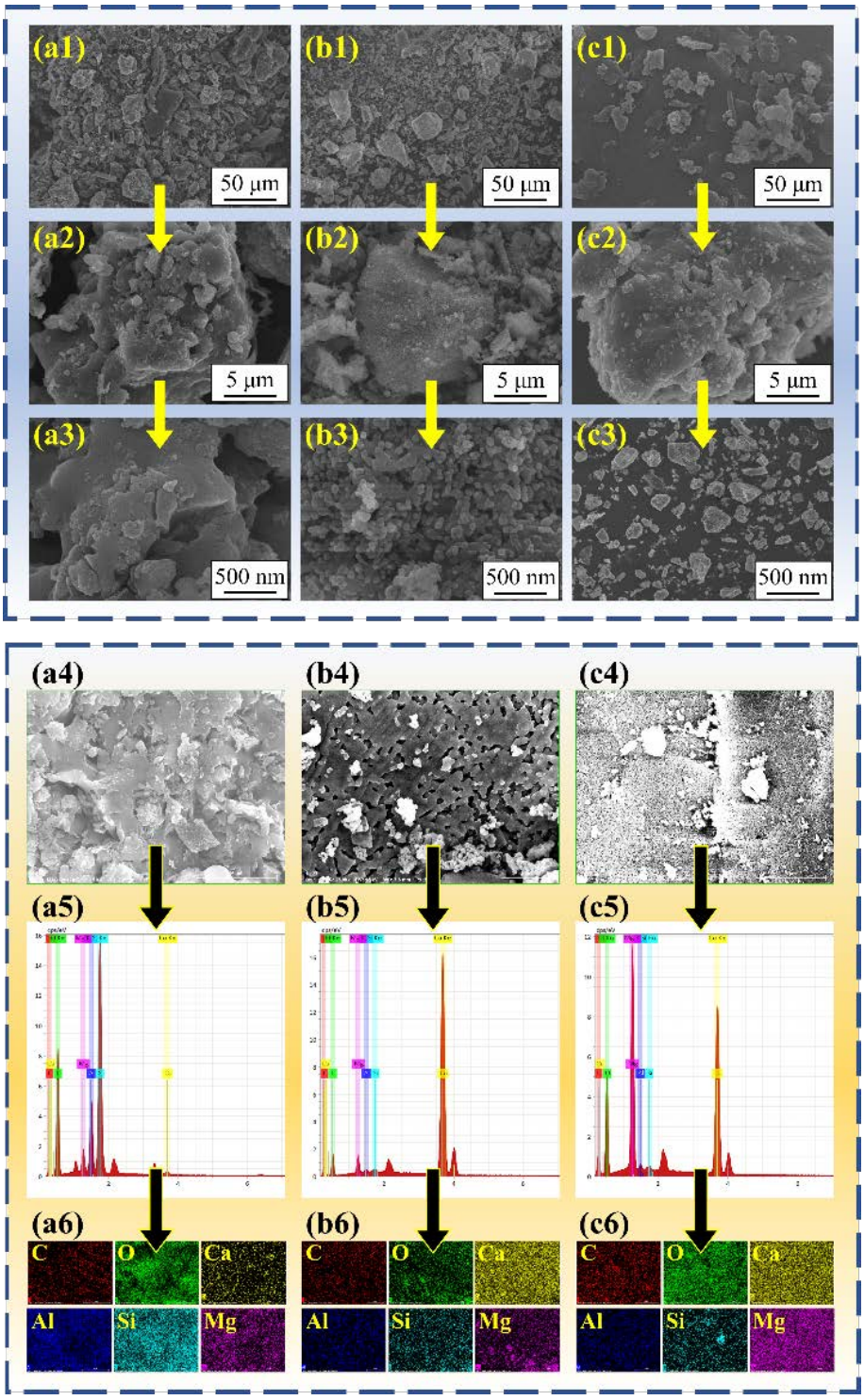

Fig. S2 SEM images and EDS mapping of (a1–6) BB900, (b1–6) DO900 and (c1–6) DO/BB.

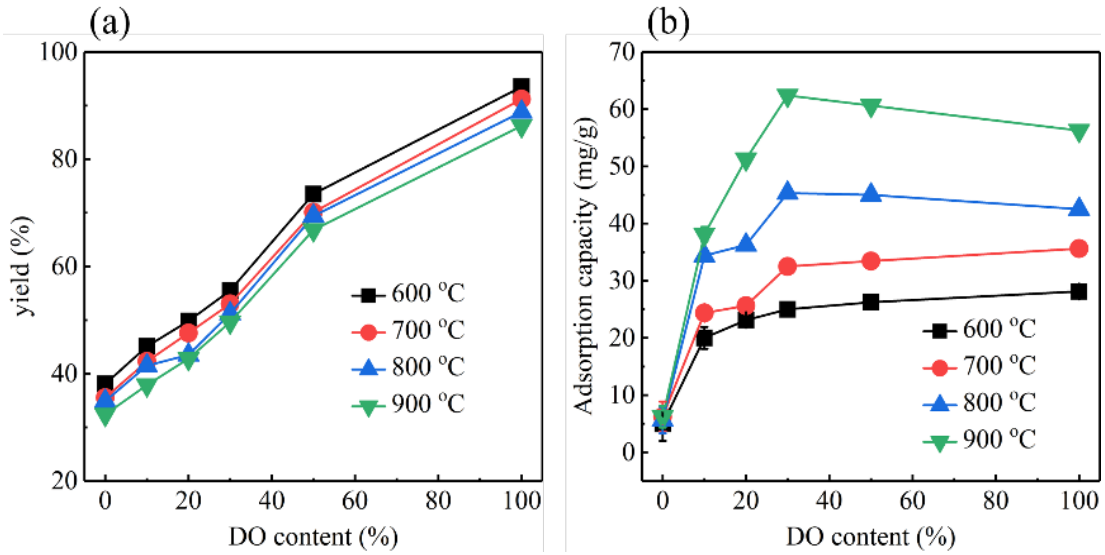

Fig. S3 (a) Yield and (b) phosphate adsorption capacity of DO/BB composite with different dolomite content and pyrolysis temperature.

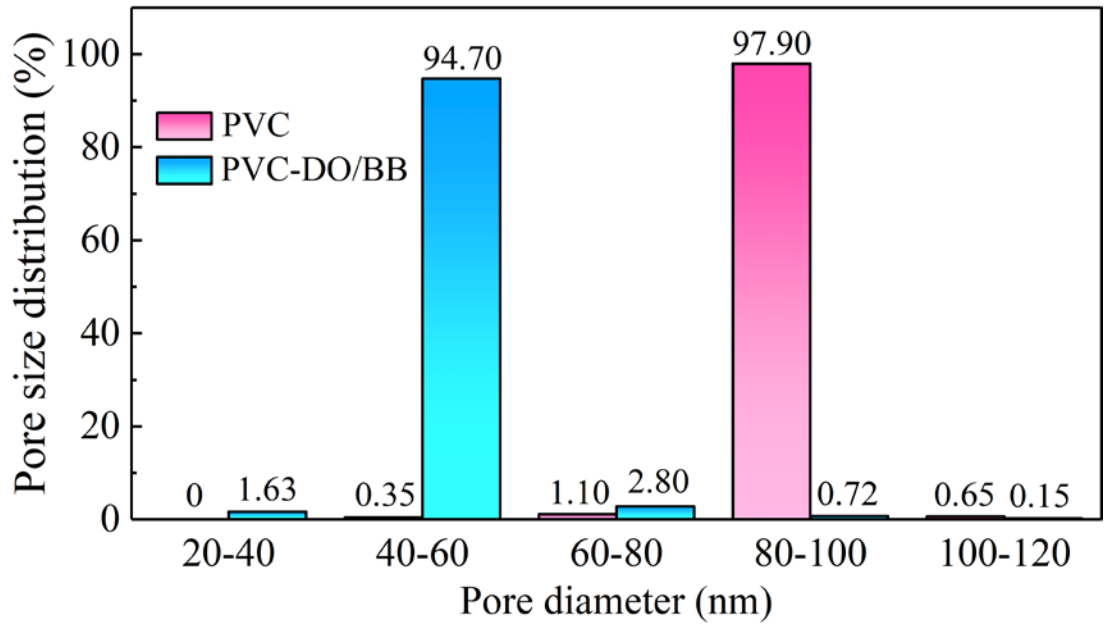

Fig. S4 Pore size distributions of PVC and PVC-20%DO/BB.

Table S1 Physical and chemical characteristics of the bentonite and dolomite.

Characteristics	Parameters	Bentonite	Dolomite
Physical characteristics	Density (g/cm^3)	2.38	2.85
	pH	8.96	9.0–10.0
	Granulometry (μm)	<11.0	<9.0
	Specific surface area (m^2/g)	32.08	/
Chemical composition (wt%)	SiO_2	63.05	7.06
	Al_2O_3	17.93	0.73
	Na_2O	4.25	0.26
	MgO	2.76	20.16
	Fe_2O_3	2.06	0.39
	MnO	1.23	/
	CaO	0.97	38.25
	FeO	0.84	/
	K_2O	0.51	/
	Br	/	5.75
	Others	6.40	27.4

Table S2 Element content of BB900, DO900 and DO/BB (wt%).

Sample	C	O	Si	Al	Ca	Mg
BB900	11.80	47.91	29.27	7.50	1.21	2.31
DO900	3.08	30.15	0.49	0.40	62.74	3.14
DO/BB	7.36	43.74	0.24	0.25	32.61	15.81

Table S3 Kinetic model parameters obtained from adsorption.

Kinetic model	Parameter	Result
pseudo-first-order	k_1 (1/h)	1.4942
	$Q_{e,cal}$ (mg/g)	27.92
	R^2	0.8907
pseudo-second-order	k_2*10^{-2} (mg/g/h)	7.263
	$Q_{e,cal}$ (mg/g)	29.96
	R^2	0.9548
Richie n_th-order	k_n ($g^{n-1}/mg^{n-1}/min$)	5.6925
	β (g/mg)	0.00
	N	4.3935
	$Q_{e,cal}$ (mg/g)	35.08
	R^2	0.9726
Elovich	α (mg/g/min)	958.09
	β (g/mg)	0.2765
	R^2	0.9921
Intraparticle diffusion	k_{i1} ($mg/g/h^{0.5}$)	21.31
	C_1 (mg/g)	0.8347
	R^2	0.9491
	k_{i2} ($mg/g/h^{0.5}$)	4.22
	C_2 (mg/g)	15.8312
	R^2	0.9567
	k_{i3} ($mg/g/h^{0.5}$)	1.07
	C_3 (mg/g)	26.2122
	R^2	0.8762

Table S4 Isotherm model parameters obtained from adsorption.

Isotherm model	Parameter	Result
Langmuir	Q_m (mg/g)	91.04
	K_L (L/mg)	10.8001
	R^2	0.6716
Freundlich	K_F ($mg^{(1-n)}\cdot L^n/g$)	70.2115
	1/n	16.1134
	R^2	0.6835
Langmuir_	Q_m (mg/g)	114.76
Fruendlich	K_{LF} (L^n/mg^n)	1.6577
	1/n	4.8657
	R^2	0.6864
Temkin	A (L/mg)	$2.48*10^7$
	B (J·g/mg)	527.77
	R^2	0.9950

References

Deng W, Zhang D, Zheng X, Ye X, Niu X, Lin Z, Fu M, Zhou S (2021). Adsorption recovery of phosphate from waste streams by Ca/Mg-biochar synthesis from marble waste, calcium-rich sepiolite and bagasse. Journal of Cleaner Production, 288: 125638

Klimaviciute R, Bendoraitiene J, Rutkaite R, Zemaitaitis A (2010). Adsorption of hexavalent chromium on cationic cross-linked starches of different botanic origins. Journal of Hazardous Materials, 181(1–3): 624–632

Luo H, Wang Y, Wen X, Cheng S, Li J, Lin Q (2021). Key roles of the crystal structures of MgO-biochar nanocomposites for enhancing phosphate adsorption. Science of the Total Environment, 766: 142618